



Binder-free Zeolite Beta Beads with Hierarchical Porosity: Synthesis and Application as Heterogeneous Catalysts for Anisole Acylation

Zahra Asgar Pour,^[a] Romar Koelewijn,^[a] Mustapha El Hariri El Nokab,^[b] Patrick C. A. van der Wel,^[b] Khaled O. Sebakhy,^[a] and Paolo P. Pescarmona*^[a]

Three zeolites (H-Beta, H-ZSM-5 and H-Y) were synthesized in the form of binder-free macroscopic beads ($d=215\text{--}840\ \mu\text{m}$) using a hydrothermal method employing anion-exchange resin beads as hard template. The beads obtained after removal of the hard template by calcination consisted of crystalline zeolite domains connected with each other to form a hierarchical porous network in which the zeolitic micropores are accessible through meso- and macropores, as proven by characterization with XRD, N_2 physisorption, SEM, and TEM. The composition, the nature and amount of acid sites and the degree of hydrophobicity of these beads were investigated by means of XRF, solid-state NMR, pyridine-FTIR and TGA. The zeolite beads were tested as heterogeneous catalysts in the Friedel-Crafts

acylation of anisole with acetic anhydride to produce para-methoxyacetophenone. H-Beta-Beads displayed the best catalytic performance with 95 % conversion of acetic anhydride and 76% yield of para-methoxyacetophenone in a batch reactor test (90°C , 6 h). Next, the catalytic performance of H-Beta-Beads was compared in both batch and continuous-flow mode to extrudates prepared by mixing zeolite Beta powder with either kaolin or bentonite binders. H-Beta-Beads outperformed the extrudates in batch-mode reactions and could be reused in multiple runs without discernible loss of activity. In the continuous-flow test, H-Beta-Beads demonstrated higher average activity but deactivated more rapidly than the extrudates.

Introduction

Friedel-Crafts acylation is a well-established route to functionalize aromatic compounds with alkanoyl groups ($-\text{COCH}_3$), thus yielding products that are widely used as building blocks in the chemical industry for manufacturing pharmaceuticals, dyes, fragrances, agrochemicals and so on.^[1–4] Conventionally, Friedel-Crafts acylations are catalyzed by homogeneous Lewis acids such as AlCl_3 or Brønsted acids such as HF. However, conducting this reaction with these homogeneous catalysts

comes with the issue of difficult separation and purification of the aromatic ketone product from the Lewis acid catalyst to obtain the final product (e.g. para-methoxyacetophenone, p-MAP, Scheme 1).^[5]

An attractive alternative to homogeneous catalysts for the acylation of aromatics is the use of zeolites as regenerable heterogeneous catalysts.^[6] Zeolites are well-known solid acid catalysts displaying a desirable combination of physicochemical properties such as crystallinity, micropores with well-defined size, tunable acidity, thermal and hydrothermal stability and high surface area.^[7–9] Additionally, they can be considered as

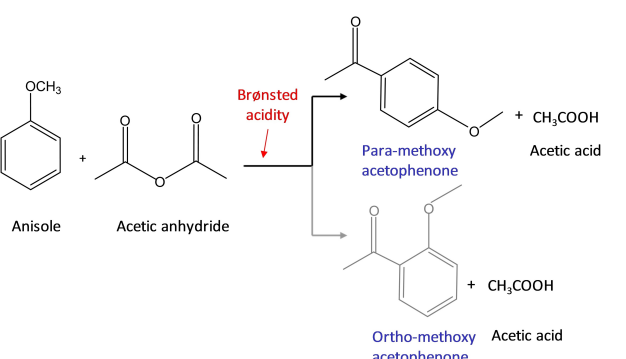
[a] Z. Asgar Pour, R. Koelewijn, Dr. K. O. Sebakhy, Prof. P. P. Pescarmona
Chemical Engineering Group
Engineering and Technology Institute Groningen (ENTEG)
University of Groningen
Nijenborgh 4
9747 AG Groningen (The Netherlands)
E-mail: p.p.pescarmona@rug.nl

[b] M. El Hariri El Nokab, Prof. P. C. A. van der Wel
Solid-State Nuclear Magnetic Resonance Group
Zernike Institute for Advanced Materials (ZIAM)
University of Groningen
Nijenborgh 4
9747 AG Groningen (The Netherlands)

 Supporting information for this article is available on the WWW under
<https://doi.org/10.1002/cctc.202200518>

 This publication is part of a joint Special Collection with EurJOC and EurJIC on the Netherlands Institute for Catalysis Research. Please see our homepage for more articles in the collection.

 © 2022 The Authors. ChemCatChem published by Wiley-VCH GmbH. This is an open access article under the terms of the Creative Commons Attribution Non-Commercial License, which permits use, distribution and reproduction in any medium, provided the original work is properly cited and is not used for commercial purposes.



Scheme 1. Catalytic route for the production of para-methoxyacetophenone (p-MAP) as the main product of anisole acylation using acetic anhydride (the acylating agent in this study). The possible formation of the by-product ortho-methoxyacetophenone (o-MAP) is shown in gray. Additionally, acetic anhydride can undergo hydrolysis into two acetic acid molecules (not shown in the scheme).

environmentally benign materials because they prevent the generation of hazardous wastes generally produced by use of homogeneous catalysts. Their inherent microporous nature ($d_p < 2 \text{ nm}$) is important as it allows zeolites to display shape selectivity, but at the same time can represent a limitation for reactions involving bulky molecules, which can encounter remarkable diffusion limitations in the micropores. In particular, such a drawback becomes more pronounced in larger zeolite crystals.^[10] In order to alleviate diffusion limitations caused by the microporous nature of zeolites, several strategies have been investigated, such as: (i) reducing the size of zeolite particles to the nanoscale; (ii) synthesizing large-pore size zeolites; or (iii) introducing hierarchical porosity in zeolites.^[11–13] The latter approach has been increasingly investigated in recent years, and is based on the formation of auxiliary larger pores (i.e. mesopores and macropores) in the zeolitic porous network.^[14,15] In order to improve the diffusion within the zeolite, it is essential that the location of these secondary pores leads to an interconnected network in which the smaller zeolitic micro-pores are accessed through larger meso- and macropores, i.e. a so-called hierarchical porous network.^[16] Hierarchical zeolites have been extensively investigated in recent decades and two main approaches have been employed for their preparation: templating or “bottom-up” and post-synthesis or “top-down” techniques.^[17–19] By using templating techniques, including hard and soft templating, mesoporosity is generated during the zeolite synthesis using hydrothermal crystallization, whereas in post-synthetic techniques secondary porosity is created in as-synthesized zeolites by controlled extraction of Al or Si from the framework.^[20–22] In general, templating techniques offer a better control of the size and location of meso- and macropores but may require harsh conditions (e.g. high temperature) and are often expensive because the template can be costly and is destroyed by combustion in the process of generating the meso- and macropores.^[23,24] On the other hand, post-synthetic techniques involve simpler procedures and are relatively inexpensive and thus considered more feasible for industrial applications. However, the Si/Al ratio and, consequently, some physicochemical properties of the zeolites are altered by partial demetallation (e.g. number of active sites, crystallinity).^[25]

Zeolites with hierarchical porosity are conventionally prepared in powder form. However, these powders would still need to be shaped into pellets to prevent pressure drop when utilized in fixed-bed reactors. For industrial application, zeolites are commonly shaped into the desired size and geometry by extrusion, in which the zeolite powder is mixed with binders such as inorganic oxides (e.g. silica or alumina) or mineral clays (e.g. kaolin or bentonite). The binder is used to impart appropriate mechanical strength against attrition and crushing. However, the presence of binders decreases the number of acid sites per unit mass and can cause partial blockage of pores as well as a decrease in specific surface area, thus affecting negatively the catalytic performance.^[26,27]

In this work, we prepared zeolites with hierarchical porosity and shaped them into macroscopic beads in a single step and without requiring a binder. To achieve this, we employed a type of macroscopic porous resin beads (Amberlite IRA-900 in Cl-

form with a size of 350 to 800 μm) as hard template. This strategy has several assets: (i) these resin beads are commercially available and inexpensive materials; (ii) they allow producing the shaped zeolite catalysts with hierarchical porosity in one step; and (iii) no binder is required, thus overcoming the above-mentioned limitations caused by the use of binders in the formulation of the shaped catalysts. This type of hard-templating technique using macroscopic resin beads was first reported for preparing Silicalite-1 beads.^[28] After that, other zeolitic frameworks in bead shape were synthesized by employing two different types of resin beads (MSA-1 and WBA) such as ZSM-5 and Beta.^[29,30] However, these studies were focused on the synthesis of these materials and no further research on their application as heterogeneous catalysts was performed.^[28–32] Amorphous titanosilicate beads (TS-1), crystalline titanosilicate beads with MFI framework and more recently Sn-Beta beads have also been synthesized and tested as heterogeneous catalysts in batch-mode reactions.^[14,33,34] Here, we report the synthesis of three zeolites frameworks in H-form and macroscopic bead format with hierarchical porosity (H-Beta-Beads, H-ZSM-5-Beads, H-Y-Beads), and their catalytic application in the acylation of anisole using acetic anhydride. None of these zeolite beads has been synthesized before using the procedure reported here, and in the case of H-Y-Beads, this is the first report of the successful synthesis of this zeolite framework in macroscopic bead format. The catalyst that gave the best performance in preliminary batch-mode tests (H-Beta-Beads) was also studied in a fixed-bed reactor set-up and compared to extrudates prepared from conventional zeolite Beta in powder form.

Results and Discussion

Three macroscopic zeolite beads with hierarchical porosity (H-Beta-Beads, H-ZSM-5-Beads, H-Y-Beads) were synthesized by hydrothermal crystallization using ion-exchange resin beads (Amberlite IRA-900) as hard template (Figure 1). These commercial polymeric beads consist of polystyrene cross-linked through the presence of divinylbenzene units and functionalized with trimethylammonium chloride groups.^[35] They are suitable as hard template for preparing zeolitic beads with spherical geometry and hierarchical porosity, owing to their high ion-exchange capacity (1 meq/mL), porous structure, stability in a wide range of pH (0–14), macroscopic size and spherical shape.^[14,35] SEM analysis of the Amberlite IRA-900 beads indicated that their size is in the 350–800 μm range (Figure 1A and B). The porous structure of these beads is characterized by irregular and mostly slit-like meso- and macropores with a wide range of openings (from 20 to 600 nm), as visualized by SEM (Figure 1C). The presence of this porosity is essential for the role of these resin beads as an appropriate scaffold for growing the zeolite crystallites. In this study, the protocol for the synthesis of zeolitic beads was developed by adapting and optimizing the original recipes used for each of the above-mentioned zeolites in conventional powder form, while including the Amberlite IRA-900 resin beads as hard template. More specifically, the

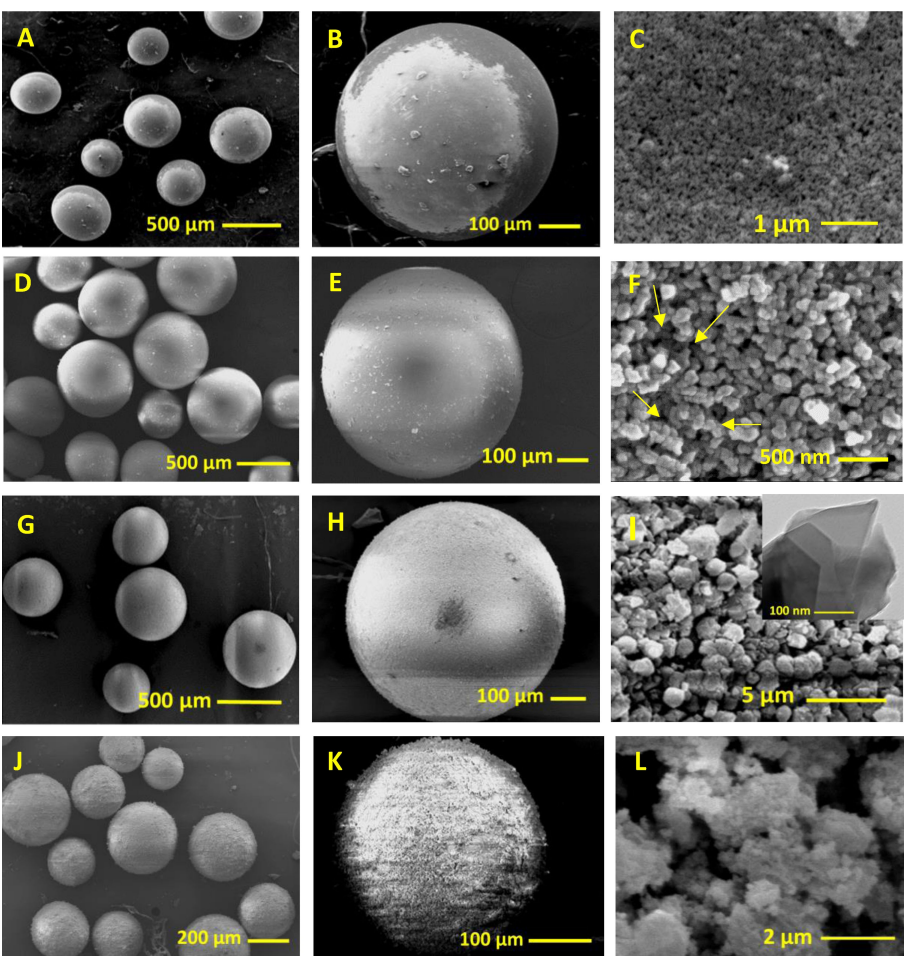


Figure 1. SEM images of: (A–C) the Amberlite IRA-900 resin beads; and (D–L) of the three zeolite beads prepared using the resin beads as hard template: (D–F) H-Beta-Beads (in the image with higher magnification, the interparticle meso- and macropores between the zeolite crystals constituting the beads are shown with yellow arrows); (G–I) H-ZSM-5-Beads (the insert of Figure 1I is a TEM image); (J–L) H-Y-Beads.

synthetic parameters were carefully optimized to maximize the degree of crystallinity in the structure of the ultimate beads. After the hydrothermal synthesis and calcination step used to remove the hard template, the physicochemical properties of the zeolite beads were thoroughly characterized using a combination of techniques. SEM images of the zeolite Beta beads showed that the obtained beads have a diameter ranging from 415 to 840 μm (Figure 1D and E) and are thus slightly larger than the original resin beads. SEM images with higher magnification proved that the beads consist of particles with an approximate size of 200–300 nm, both at the surface (Figure 1F) and in the bulk of the bead (Figure S5A).^[30] XRD analysis of the beads showed all characteristic peaks of zeolite Beta [BEA] (Figure 2A), thus proving that the particles that constitute the beads consist of Beta zeolite crystals. The XRD peaks had slightly lower signal-to-noise ratio compared to the zeolite Beta in powder form (H-Beta-Pow) that was obtained as side-product during the synthesis of H-Beta-Beads (Figure 2A). No additional signal was detected in the XRD patterns, indicating the presence of a single crystalline phase. The SEM images also showed that the crystalline zeolite particles are interconnected

to each other, thus generating a hierarchical porous structure in which the zeolitic micropores are accessible through a network of interparticle meso- and macropores (Figures 1F and S5A). The size and crystalline lattice of the zeolite particles and the interparticle porosity were confirmed by TEM analysis (Figure 3A and B). Such interparticle porosity is anticipated to promote the diffusion of reactants and products through the beads in their catalytic application.^[36]

The ZSM-5-Beads display a size close to that of the H-Beta-Beads (see SEM images in Figure 1G and H). On the other hand, the particles of which the H-ZSM-5-Beads consist are significantly larger, having an average size in the 0.5–1 μm range (Figure 1I). The crystalline nature of these particles was demonstrated by XRD (Figure 2B). TEM and SEM analysis indicate that these particles consist of aggregates of zeolite crystals (Figure 3C and D and insert of Figure 1I).^[37,38] The particle size of a zeolite catalyst plays a crucial role in the mass transfer during the catalytic reaction, and the larger size of the particles of which H-ZSM-5-Beads are made compared to those in H-Beta-Beads is potentially a pitfall for mass diffusion and consequently for catalytic performance,^[39] particularly for reactions involving

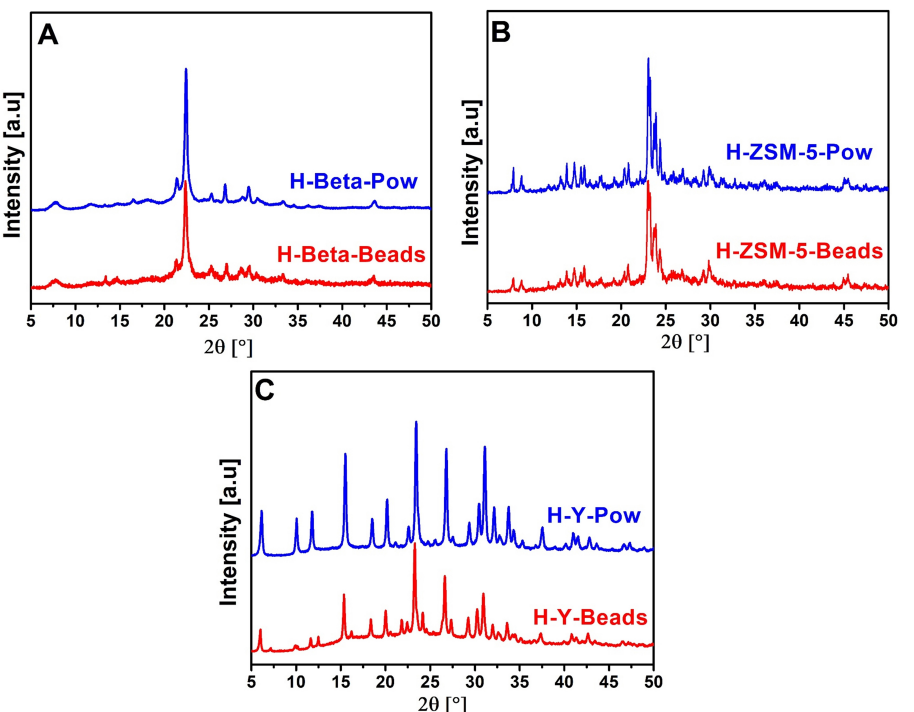


Figure 2. XRD pattern of zeolite samples after calcination: (A) H-Beta-Pow and H-Beta-Beads; (B) H-ZSM-5-Pow and H-ZSM-5-Beads; (C) H-Y-Pow and H-Y-Beads. The XRD patterns of the materials in powder form are shown in blue, those of the beads are shown in red.

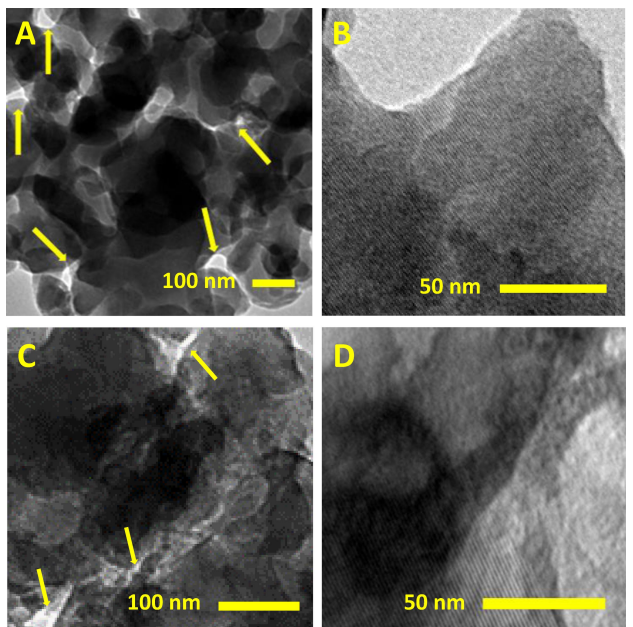


Figure 3. TEM images of zeolite beads: (A–B) H-Beta-Beads; (C–D) H-ZSM-5-Beads (the meso-and macropores are indicated with yellow arrows).

bulky molecules such as the anisole acylation studied in this work. Similar to what was observed in H-Beta-Beads, the zeolite crystalline particles are interconnected to form a porous network (Figure 1I and 3 C and D).

While our synthesis methods were efficient for preparing beads consisting of crystalline zeolite Beta and ZSM-5, obtaining a material with similar quality for zeolite Y proved difficult. Even after careful optimization of the synthesis by including aging the zeolite precursor solution for 7 days at room temperature and a two-step temperature program in the hydrothermal crystallization step (see experimental section), the H-Y-Beads displayed lower crystallinity compared to their counterpart in powder form (Figure 2C). Additionally, the XRD pattern of H-Y-Beads displayed a broad peak between $20 = 15^\circ$ and 35° , which is characteristic of amorphous SiO_2 (Figure 2C).^[40] Although prolongation of the above-mentioned aging time up to 7 days allowed minimizing the intensity of this broad peak, we could not achieve zeolite Y beads that did not show the signal of amorphous silica in their XRD pattern. This is a clear difference compared to H-Beta-Beads and H-ZSM-5-Beads, which do not show a notable signal in the same region of the XRD pattern (Figure 2A and B), indicating that they contain, if any, a much lower fraction of amorphous silica. SEM images of the H-Y-Beads showed shrinkage in size compared with the resin beads (Figure 1J and K), which is the opposite trend to what observed with the other two zeolite beads. The degree of dimensional shrinkage was larger in samples with large content of amorphous silica (not presented in more detail here), to the extent of being observable by naked eye. SEM images with higher magnification indicated that the beads consist of aggregates of relatively small particles (Figure 1L), which differ significantly from the large octahedral crystals that characterize

Table 1. Physicochemical properties of the catalysts in powder, bead or extrudate format used in the acylation of anisole.

Entry	Material	Specific surface area [m ² /g] ^[a]	Micropore volume [cm ³ /g]	Meso-/macro pore volume [cm ³ /g] ^[b]	Meso/macro pores size [nm]	Si/Al molar ratio [XRF] ^[c]	Si/Al molar ratio [NMR] ^[d]	Na/Al molar ratio [XRF] ^[c]	Adsorbed H ₂ O ^[e] [n _{H₂O} /nm ²]
1	H-Beta-Beads	566	0.20	0.28	5–100	9.8	13	0.17	8.0
2	H-Beta-Pow	521	0.18	—	—	13	13	0	10.5
3	H-ZSM-5-Beads	329	0.11	0.13	5–80	12	16	0	7.6
4	H-ZSM-5-Pow	287	0.10	—	—	15	17	0	8.3
5	H-Y-Beads	508	0.15	0.32	5–80	1.7	1.6	0.48	7.3
6	H-Y-Pow	486	0.15	—	—	2.9	3.0	0.48	10.3
7	H-Y-Beads-SC	478	0.15	0.16	5–100	8.8	n.d.	0	n.d.
8	Beta90Kao10-Extr	491	0.15	0.71	>50 (mainly)	9.8	n.d.	0	n.d.
9	Beta70Kao30-Extr	409	0.12	0.64	>50 (mainly)	5.2	n.d.	0	9.9
10	Beta50Kao50-Extr	278	0.08	0.47	>50 (mainly)	3.4	n.d.	0	10.8
11	Beta90Ben10-Extr	477	0.14	0.73	>50 (mainly)	12	n.d.	0	n.d.
12	Beta70Ben30-Extr	397	0.11	0.59	>50 (mainly)	8.7	n.d.	0	n.d.
13	Beta50Ben50-Extr	275	0.08	0.44	>50 (mainly)	6.4	n.d.	0	n.d.
14	Pure kaolin	9	—	0.06	—	n.d.	n.d.	n.d.	n.d.
15	Pure bentonite	3	—	0.08	—	n.d.	n.d.	n.d.	n.d.

[a] BET surface area, [b] BJH cumulative pore volume between 1.7 and 300 nm width, based on the desorption branch of the isotherm, [c] Determined by XRF, [d] Si/Al molar ratio calculated from ²⁹Si MAS NMR (with an estimated error of 5–10% due to peak overlap, which complicates the peak deconvolution process), [e] Calculated based on the mass loss of the sample between 25 and 300 °C as determined by TGA. n.d.: not determined.

the zeolite Y counterpart prepared in powder form (Figure S5B).^[41]

The textural properties of the zeolitic beads and powders were investigated by N₂ physisorption (Table 1). All the three zeolite beads exhibited a type IV isotherm (Figure 4) with a hysteresis loop at large p/p⁰ values (>0.9). This hysteresis loop is attributed to the so-called bottleneck effect of connected meso- and macropores.^[42] The pore-size distributions for the zeolitic beads were broad (Figure S6). It is worth noting that also the physisorption isotherms of zeolite Beta and zeolite Y in powder form presented a narrow hysteresis loop at large p/p⁰ values (Figure S7), which is attributed to the presence of interparticle voids generated by particles agglomeration. H-Beta-Beads showed the highest specific surface area (566 m²/g) among all the zeolitic materials prepared in this work, and all zeolitic beads showed higher surface area compared with their

powder counterparts (Table 1, entries 1–6). The micropores volume of all zeolite bead samples were very similar to those of their powder counterparts (Table 1, entries 1–6).

The ²⁹Si MAS NMR spectra of zeolite Beta beads and powder showed a similar signal (Figure 5A), consisting of: (i) a peak centered at δ = -111 ppm, which is characteristic for Si(0Al), i.e. a Si atom in a tetrahedral SiO₄ unit surrounded by 4 other Si atoms; and a partially overlapping peak centered at around δ = -103 ppm, which is related to Si(1Al), i.e. a Si atom in a tetrahedral SiO₄ unit with 1 Al and 3 Si atoms as neighbors. The ²⁹Si MAS NMR spectra of ZSM-5 beads and powder also displayed a similar signal as that observed in the case of the zeolite Beta samples, though the Si(1Al) peak is centered at around δ = -105 ppm (Figure 5B). On the other hand, the ²⁹Si MAS NMR spectra of H-Y-Pow and H-Y-Beads displayed a more complex signal (Figure 5C) compared to the other zeolites. This is a consequence of the higher Al content of zeolite Y, which for

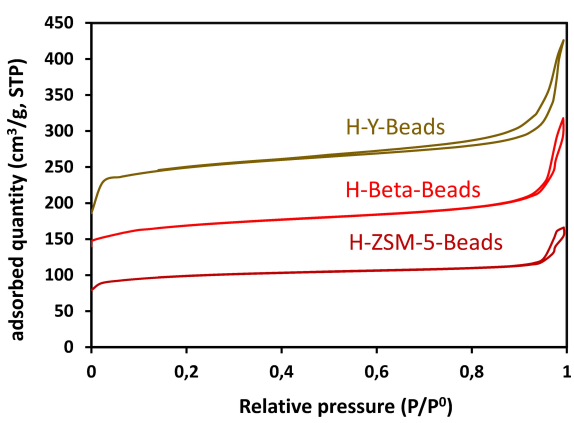


Figure 4. N₂ physisorption isotherms of the zeolite beads (for the sake of readability, the isotherm of H-Y-Beads has been shifted up of 100 cm³/g along the vertical axis).

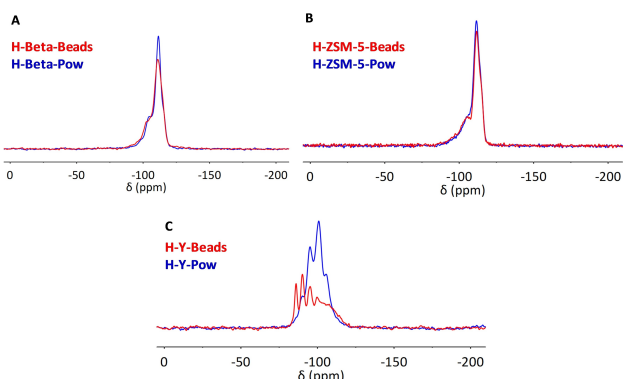


Figure 5. ²⁹Si MAS NMR spectra of: (A) H-Beta-Beads and H-Beta-Pow; (B) H-ZSM-5-Beads and H-ZSM-5-Pow; (C) H-Y-Beads and H-Y-Pow.

H-Y-Pow led to four peaks at $\delta = -106, -100, -94$, and -90 ppm, corresponding to Si(0Al), Si(1Al), Si(2Al) and Si(3Al), respectively;^[43] and to five peaks for H-Y-Beads at $\delta = -106, -97, -93, -88$, and -83 ppm corresponding to Si(0Al), Si(1Al), Si(2Al), Si(3Al) and Si(4Al), respectively. The relative intensity of the peaks corresponding to Si with a large number of Al neighbors was notably higher for zeolite Y in bead format compared to the powder counterpart (Figure 5C). Based on these ^{29}Si MAS NMR data, it was possible to estimate the Si/Al ratio for all bead and powder samples (Table 1). The obtained Si/Al values are in good agreement with those obtained by means of XRF analysis (Table 1). In general, a slightly lower Si/Al ratio was observed for beads compared to the corresponding powder (Table 1).

The ^{27}Al MAS NMR of the zeolite Beta, ZSM-5 and Y samples showed one peak at around $\delta = 55$ ppm (H-Beta and H-ZSM-5) or 60 ppm (H-Y), which originates from tetrahedrally coordinated Al atoms as expected for Al sites incorporated in the zeolite framework (Figure 6). These tetrahedral Al sites are associated with the Brønsted acidity that is characteristic of aluminosilicate zeolites in their H-form. A second peak was observed at $\delta = 0$ ppm, which is characteristic for extra-framework Al species in octahedral coordination.^[43] This type of extra-framework Al species is often observed in Al-rich zeolites.^[44–46] Notably, the intensity of this peak relative to the peak of tetrahedral Al was higher in the zeolite powders than in their bead analogs. This result might indicate a more efficient incorporation of Al in the zeolitic framework in the beads compared to the powders, or might stem from a more efficient removal of the extra-framework Al species from the hierarchically porous structure of the beads during the washing steps that were carried out after the hydrothermal synthesis of these materials.

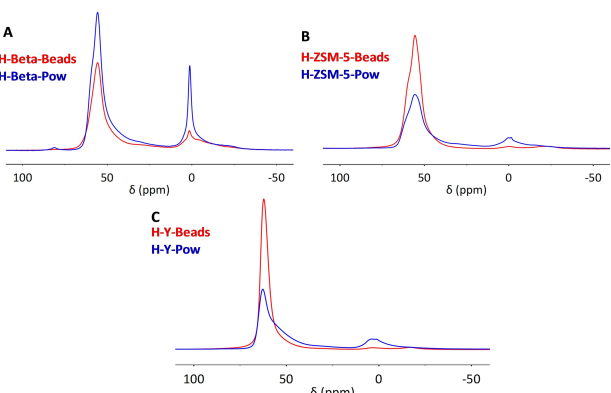


Figure 6. ^{27}Al MAS NMR spectra of: (A) H-Beta-Beads and H-Beta-Pow; (B) H-ZSM-5-Beads and H-ZSM-5-Pow; (C) H-Y-Beads and H-Y-Pow.

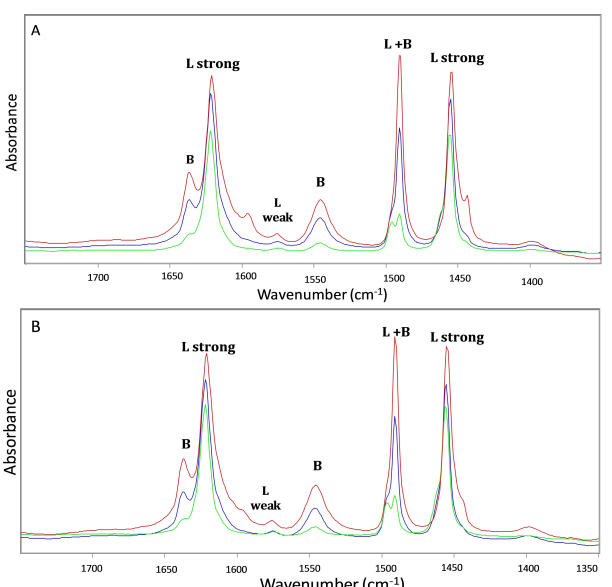


Figure 7. FT-IR spectra of pyridine adsorbed at 150°C (red), 250°C (blue) and 450°C (green) on (A) H-Beta-Pow and (B) H-Beta-Beads.

In order to evaluate the type and strength of acid sites in the zeolite Beta samples (as the most active catalysts in this study, *vide infra*), FTIR analysis of adsorbed pyridine was carried out at $150, 350$ and 450°C (Figure 7). The characteristic bands in the range of $1430\text{--}1475\text{ cm}^{-1}$ that correspond to pyridine adsorbed on Lewis acid sites, and between $1515\text{--}1565\text{ cm}^{-1}$ for pyridine adsorbed on Brønsted acid sites were integrated for the above-mentioned temperatures and the results are shown in Table 2.^[47] At all three temperatures, the amount of Lewis acid sites was higher than that of Brønsted acid sites. This feature has been observed before in Beta zeolites with relatively low Si/Al (as in our case) and is likely due to the presence of extra-framework Al species in these samples (also detected by ^{27}Al MAS NMR, Figure 6A).^[44–46] In addition, the ratio between Lewis and Brønsted acidity increased by increasing the temperature, indicating the milder nature of the Brønsted acid sites compared with the Lewis acid sites. Furthermore, at all temperatures, the powder sample displayed higher total acidity (Table 2). This is attributed to the presence of residual Na in the H-Beta-Beads sample (as evidenced by XRF, see Table 1, entry 1), which indicates that the ion-exchange step to convert this zeolite into its H-form was incomplete. Additionally, the lower degree of crystallinity of H-Beta-Beads compared to H-Beta-Pow (*vide supra*) might imply that some Al sites in tetrahedral coordination but in an amorphous domain display too low acidity and thus too weak adsorption of pyridine to be

Table 2. Type and amount of surface acid sites of the zeolite Beta samples in powder and bead format.

Catalyst	Brønsted acidity [mmol g^{-1}]			Lewis acidity [mmol g^{-1}]			Lewis/Brønsted acid ratio		
	150°C	350°C	450°C	150°C	350°C	450°C	150°C	350°C	450°C
H-Beta-Pow	0.171	0.070	0.026	0.298	0.221	0.186	1.74	3.16	7.15
H-Beta-Beads	0.123	0.070	0.018	0.206	0.158	0.141	1.67	2.26	7.83

detected by FTIR. It should be noted that both Brønsted and Lewis acid sites have been reported to be able to catalyze the acylation of anisole.^[48,49] The generally accepted mechanism involves the formation of an acylium ion from acetic anhydride (promoted by either type of acid), followed by attack of the acylium ion on the aromatic ring.^[6]

In order to analyze the hydrophilicity of our catalysts, thermogravimetric analysis (TGA) was carried out on all zeolites in bead and powder format (Figure S4). These data allowed estimating the amount of water molecules adsorbed per nm² of each material (Table 1). While the H-ZSM-5 zeolites are relatively hydrophobic in line with their relatively low Al content, the H-Beta zeolites displayed similar yet higher hydrophilicity than the H-Y zeolites, despite the higher Al content of the latter. The relatively higher hydrophilicity of the H-Beta materials could be caused by a larger population of silanol groups on the external surface of the zeolite particles,^[50] which would promote water adsorption but would be expected to have no or minor influence on the catalytic activity, which occurs mainly within the zeolite pores. It is worth noting that for each zeolite framework type, the material in bead format displayed lower hydrophilicity compared to the powder sample. This might be attributed to the condensation between the zeolite crystals that form the walls of the beads, which would imply a lower population of hydrophilic silanol groups on the external surface of the crystals compared to the discrete particles in the powder sample.

Catalytic performance of zeolite beads and powders in the acylation of anisole in batch mode

The catalytic performance of the zeolite beads in the Friedel-Crafts acylation of anisole using acetic anhydride as acylation agent (Scheme 1) was investigated initially in batch reactors. Based on the characterization study (*vide supra*), the beads have several attractive features for this catalytic application: (i) they have a macroscopic bead format that allows their easy separation from the reaction mixture by spontaneous settling upon stopping of the stirring, without any need for filtration or centrifugation; (ii) they consist of interconnected zeolite crystals

in their H-form (acid sites), which can be accessed through a network of meso- and macropores that is expected to improve the mass diffusion and increase the accessibility to the active sites within the zeolitic micropores. In order to determine suitable reaction conditions for the catalytic acylation of anisole, the effect of temperature and mass of catalyst were investigated in a series of preliminary tests using H-Beta-Pow and H-Beta-Beads (Table S1 and S2). Based on the obtained results, 90 °C and 0.25 g of catalyst were found to give the highest selectivity and yield and were selected for further study. It is worth noting that the chosen reaction temperature (90 °C) is relatively mild compared to previous catalytic studies for this reaction (see Table S3).^[51] Afterwards, the different catalytic beads (H-Beta-Beads, H-ZSM-5-Beads, H-Y-Beads) were tested in the acylation of anisole in batch mode and their performance was compared with the corresponding materials in powder format (H-Beta-Pow, H-ZSM-5-Pow, H-Y-Pow). Among all tested catalysts, H-Beta-Pow and H-Beta-Beads demonstrated the best catalytic performance in terms of acetic anhydride conversion ($\geq 95\%$) and selectivity toward p-MAP (80–83 %), with the zeolite in powder format performing slightly better than the beads (Table 3, entry 1 and 2), in agreement with the largest population of acid sites observed by FTIR of adsorbed pyridine for the powder sample (Table 2). The better performance of zeolite H-Beta compared with H-ZSM-5 and H-Y (higher conversion and p-MAP yield achieved in a shorter reaction time) is consistent with previous studies,^[49,52–56] and is attributed to the specific pore architecture of zeolite Beta having large, intersecting channels defined by 12-membered rings.^[39,52,56,57] For the H-Beta Beads catalyst we conducted a kinetic test (Figure 8A), which allowed us to determine the Conv._{acetic anhydride} (25 %) and Yield_{p-MAP} (14 %) after 25 min of reaction, and thus to determine the initial reaction rate (see SI for details). Based on these data, we used the Weisz-Prater criterion to estimate whether internal mass transfer inside the beads limited the reaction rate. The calculated Weisz-Prater number (C_{WP}) is $\ll 1$ (see SI for details), which indicates that the reaction is not limited by internal diffusion in the bead-shaped catalyst. While H-Beta-Pow slightly outperformed H-Beta-Beads, the trend with the H-ZSM-5 catalysts was the opposite: H-ZSM-5-Pow displayed only 9 % conversion after 16 h and no acylation product was

Table 3. Catalytic performance of zeolitic powders and beads in the batch-mode acylation of anisole.^[a]

Entry	Catalyst	Anisole/ acetic anhydride molar ratio	Reaction time [h]	Acetic anhydride Conv. [%] ^[b]	p-MAP Yield [%]	p-MAP Sel. [%]	o-MAP Sel. [%]	Hydrolysis of acetic anhydride Sel. [%]
1	H-Beta-Beads	5:1	6	95	76	80	0	20
2	H-Beta-Pow	5:1	6	100	83	83	0	15
3	H-ZSM-5-Beads	5:1	16	18	4	24	0	76
4	H-ZSM-5-Pow	5:1	16	9	0	0	0	100
5	H-Y-Beads	5:1	20	37	0	0	0	100
6	H-Y-Pow	5:1	20	31	0	0	0	100
7	H-Y-Bead-SC	5:1	6	36	18	49	0	51

[a] Reaction conditions: anisole = 50 mmol, acetic anhydride = 10 mmol, mesitylene (as internal standard) = 25 mmol, catalyst mass = 0.25 g, temperature = 90 °C. [b] The conversion was measured based on acetic anhydride, as this is the limiting reactant with the employed 5:1 ratio between anisole and acetic anhydride.

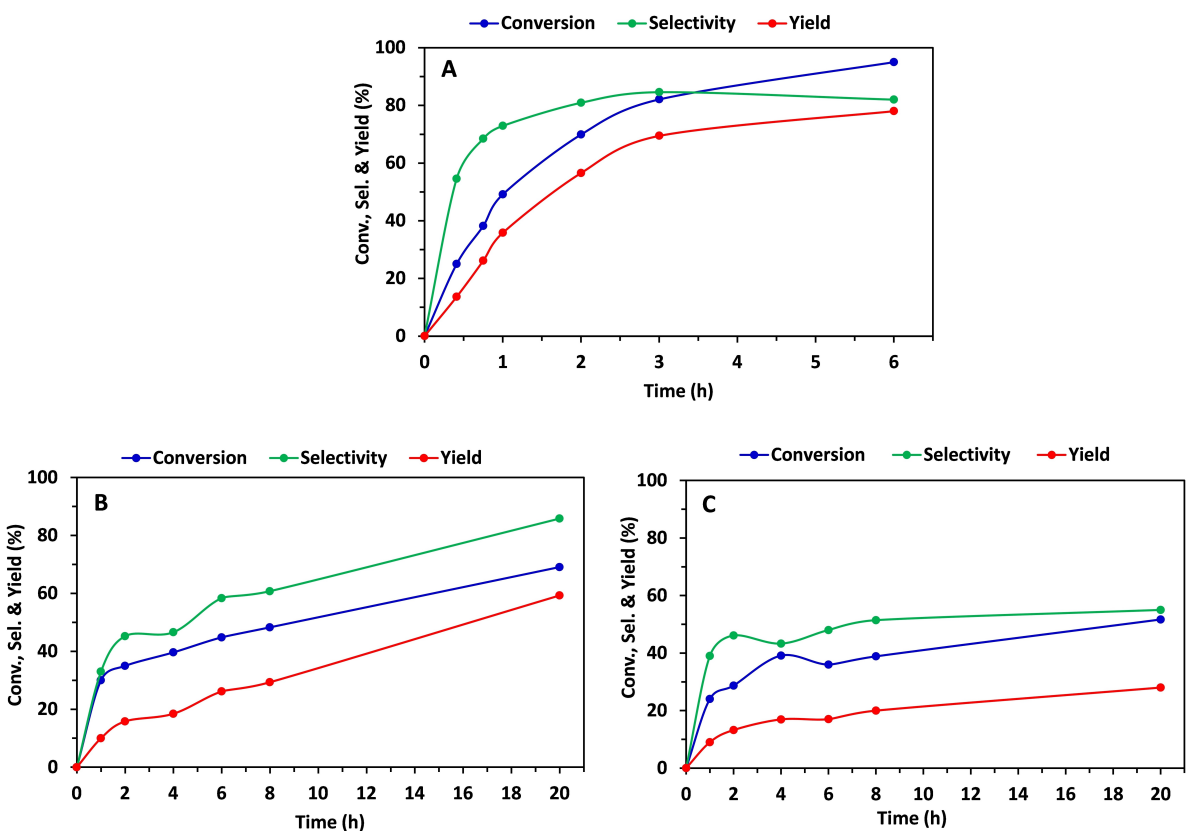


Figure 8. Kinetic study: (A) over H-Beta-Beads, temperature = 90 °C, catalyst mass = 0.25 g, anisole = 50 mmol, acetic anhydride = 10 mmol (anisole to acetic anhydride molar ratio = 5:1); (B) over H-ZSM-5-Beads, temperature = 100 °C, catalyst mass = 0.25 g, anisole = 40 mmol, acetic anhydride = 5 mmol, (anisole to acetic anhydride molar ratio = 8:1); (C) over H-Y-Beads-SC, temperature = 90 °C, catalyst mass = 0.25 g, anisole = 50 mmol, acetic anhydride = 10 mmol (anisole to acetic anhydride molar ratio = 5:1).

detected in this test (Table 3, entry 4), whereas H-ZSM-5-Beads exhibited 18% conversion of acetic anhydride and 24% selectivity toward p-MAP, resulting in a final yield of 4% after 16 h (Table 3, entry 3). This result highlights the influence of the hierarchical porosity of H-ZSM-5-Beads on improving the catalytic performance of this zeolite, whose micropores (10-membered rings) are significantly smaller and thus more prone to steric and diffusion limitations than those of zeolite Beta.^[54,57–60] With the purpose of enhancing the yield of the acylation reaction over H-ZSM-5-Beads, we performed a kinetic study using a higher anisole to acetic anhydride ratio (8:1) and a higher reaction temperature (100 °C). In this test, a maximum acetic anhydride conversion of 69% was reached after 20 h, with the final p-MAP yield being 59% (Figure 8B). The increase in the selectivity towards the acylation product with increasing conversion of acetic anhydride that was observed in the kinetic tests (Figure 8) is probably due to the gradual increase in the molar ratio between anisole and acetic anhydride as the reaction proceeds (from the initial 8:1 to a theoretical 15:1 at 50% conversion of acetic anhydride). A higher ratio is expected to enhance the probability of acetic anhydride to react with anisole rather than to undergo hydrolysis, thus leading to the observed trend of increasing selectivity. In the case of zeolite Y, no acylation product was observed for either H-Y-Beads or H-Y-Pow after 20 h and only conversion of acetic anhydride by

hydrolysis into acetic acid was observed (37% and 31%, respectively, see Table 3, entries 5 and 6). This poor catalytic performance is ascribed to the inefficient conversion of the original Na-Y zeolites into their H-form by ion-exchange, as indicated by the high Na/Al ratio (0.48) of these materials measured by XRF (Table 1, entries 5 and 6), which implies a much lower population of acid sites than what would be expected for a Y zeolite fully in H-form. Additionally, these samples display relatively low crystallinity (*vide supra*), which means that some Al sites in tetrahedral coordination are in an amorphous domain and thus display lower acid strength compared to those in crystalline zeolitic domains. Furthermore, H-Y-Pow showed a highly hydrophilic nature (based on TGA, see Table 1, entry 6), which might hinder diffusion of the relatively apolar anisole. Although H-Y-Beads or H-Y-Pow showed to be poor catalysts for the acylation of anisole, a batch of catalytic beads synthesized in the absence of TMA⁺ as SDA and possessing lower crystallinity (H-Y-Beads-SC) gave 36% conversion of acetic anhydride, with 49% selectivity toward p-MAP after 6 h of reaction (Table 3, entry 7). This catalytic behavior is likely due to the fact that this zeolite does not contain Na and is fully in H-form (Table 1, entry 7), indicating that a larger fraction of the Al sites generates Brønsted acid centers. Additionally, H-Y-Beads-SC displayed a higher Si content (Si/Al = 9) compared to H-Y-Beads, which implies that

H-Y-Beads-SC is a less hydrophilic material. H-Y-Beads-SC showed better catalytic performance than H-ZSM-5-Beads (Table 3, compare entries 3 and 7). This is ascribed to its large 12-member ring pores with sodalite type cavities and considerably higher specific surface area, which increase the accessibility to the active sites (Table 1, entries 3 and 7). A kinetic test was performed for H-Y-Bead-SC at 90 °C for 20 h: the conversion of acetic anhydride reached 29% after 2 h and then gradually increased to 52% after 20 h (Figure 8C). However, this is still much lower than the catalytic activity displayed by H-Beta-Beads after only 6 h (Table 3, entry 1), in line with the lower activity of zeolite H-Y compared to zeolite H-Beta reported in the literature.^[49,52,53,56] It is worth noting that the color of H-Beta-Beads changed to dark brown by the end of the 6 h reaction (Figure S8A), whereas the color of H-ZSM-5-Beads and H-Y-Beads-SC after running the reaction for 20 h was also brown (Figure S8B-C), but significantly lighter than in the case of H-Beta-Beads. The same trend in darkening of the zeolite catalysts was observed for the powder samples. The fact that the degree of darkening seems correlated to the degree of conversion of acetic anhydride indicates that some of the reaction products (possibly oligomeric species) tend to adsorb on the catalyst surface.^[61] To quantify the adsorption of carbonaceous compounds on different catalysts, we conducted TGA analysis (30 to 800 °C in air) on selected used catalysts (H-Beta-Pow, H-Beta-Beads, H-Y-Beads and H-ZSM-5-Beads, see Figure S9). The mass loss below 200 °C is related to removal of adsorbed water, whereas the amount of carbonaceous residues was estimated from the mass loss above 200 °C. As anticipated, the amount of carbonaceous deposit was higher for the most active catalysts (13.1 wt % for H-Beta-Beads and 12.5 wt % for H-Beta-Pow) compared to the other zeolites (9.1 wt % for H-Y-Beads-SC and 8.6 wt % for H-ZSM-5-Beads). It should be noted that the mass of adsorbed carbonaceous species corresponds to 0.3–0.5% of the mass of the organic reactants used in each catalytic test (Figure S9) and thus does not affect the carbon balance of these reactions, which was nearly complete in all cases.

Comparison between zeolite Beta powder, beads and extrudates as catalysts for the acylation of anisole in batch mode

Zeolite Beta, either in powder or bead format, was identified as the most promising catalyst for the acylation of anisole among the different zeolites that were tested. Therefore, this zeolite framework was selected for further study. With the purpose of comparing our binder-free H-Beta-Beads with a conventional pelletized catalyst, we prepared extrudates by mixing H-Beta-Pow with kaolin or bentonite as binder (10 to 50 wt % of binder). Kaolin and bentonite were selected for this purpose as these clays are often used as binders in industrial pellets.^[26,62] The specific surface area and pore volume of these lab-made extrudates were analyzed using N₂ physisorption and showed a decreasing trend by increasing the mass ratio of kaolin or bentonite binder (Table 1, entries 8–13). The decrease in the micropore volume is attributed to the lack of micropores in the

binder and to partial blocking of the entrance of the zeolitic micropores by the binder, whereas the drop in surface area of the extrudates is due to the low specific surface area of the two clays used as binders (Table 1, Entry 14 and 15). While the micropore volume and the specific surface area of the extrudates were inferior to that of the binder-free H-Beta-Beads and of H-Beta-Pow, the values of the meso/macropore volumes were significantly higher compared with H-Beta-Pow and H-Beta-Beads (Table 1, entries 1 and 2 and 8–13). The latter feature is attributed to the larger particles of the clays compared with the zeolite particles as visualized by SEM images (compare Figure 9, A and B, with Figures 1F and S5A). This hypothesis is supported by the SEM images of the extrudates (Figure 9C and D), which highlight how the plate-like particles of clay are mixed with the smaller zeolite particles forming a composite with large pores.^[26] Elemental analysis by XRF indicated that the Al content of the extrudates increased with the relative amount of clay, in agreement with the fact that both kaolin and bentonite have much lower Si/Al ratio compared to zeolite Beta.^[63]

The performance of the extrudates as catalysts for the acylation of anisole was compared to that of H-Beta-Beads and H-Beta-Pow under more challenging conditions than those that were employed in the tests performed in the first part of this work (e.g. using shorter reaction time and a lower loading of catalyst relative to anisole and acetic anhydride, see Table 4). Under these conditions, only intermediate conversions are obtained (Table 4), which allows highlighting better the differences in activity between the catalysts. Compared with H-Beta-Pow as the reference catalyst, the extrudates displayed lower activity, with the decrease being monotonically correlated with the increase in binder content (Table 4, entry 1 and 3–8). This trend can be attributed to the expected lack of active sites in the clays used as binder^[62–64] and, to a lesser extent, to the observed decrease in surface area and to the possible ion exchange of alkali metals present in the clays with the Brønsted acid sites of the zeolite, leading to their neutralization.^[62–64] Bentonite-containing extrudates displayed slightly lower activity than their kaolin-containing counterparts, which can be

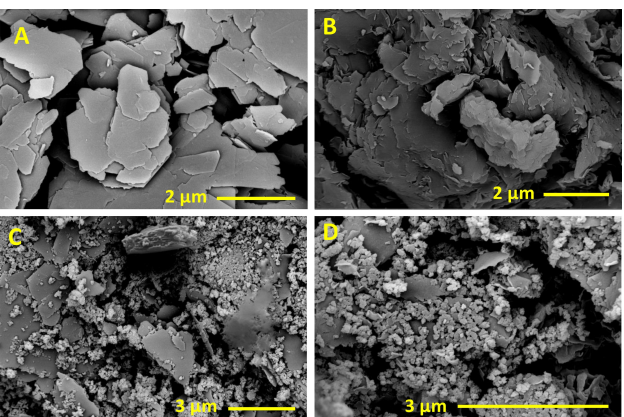


Figure 9. SEM images of: (A) Pure kaolin; (B) Pure bentonite; (C) Beta50-Kao50-Extr; (D) Beta50Ben50-Extr.

Table 4. Activity of powder and shaped zeolite Beta catalysts in the batch-mode acylation of anisole.^[a]

Entry	Catalyst	Acetic anhydride Conv. [%] ^[b]	p-MAP Yield [%]	p-MAP Sel. [%]	o-MAP Sel. [%]	Hydrolysis of acetic anhydride Sel. [%]
1	H-Beta-Pow	59	41	70	0	30
2	H-Beta-Beads	42	22	52	0	46
3	Beta90Kao10-Extr	41	19	47	0	53
4	Beta70Kao30-Extr	38	18	47	0	53
5	Beta50Kao50-Extr	32	14	43	0	57
6	Beta90Ben10-Extr	40	20	49	0	51
7	Beta70Ben30-Extr	36	14	40	0	60
8	Beta50Ben50-Extr	23	5	21	0	79

[a] Reaction conditions: anisole = 25 mmol, acetic anhydride = 5 mmol, mesitylene (as internal standard) = 12.5 mmol, catalyst mass = 0.03 g, reaction time = 2.5 h, temperature = 90 °C. [b] The conversion was measured based on acetic anhydride, as this is the limiting reactant with the employed 5:1 ratio between anisole and acetic anhydride.

attributed to their slightly lower surface area (Table 1, entries 8–13). On the other hand, H-Beta-Beads showed to be more active than the extrudates because it consists of zeolite Beta crystallites that are not diluted by the presence of binders and owing to its higher surface area. This result demonstrates the benefit of preparing the catalysts in the format of binder-free zeolite beads.

The reusability of H-Beta-Beads and H-Beta-Pow was evaluated in 4 consecutive runs in batch mode (Figure 10). Although some fluctuations in activity were observed in these recycling tests, the overall trend is that the activity of both catalysts was preserved upon reuse, as particularly clear when comparing the activity of H-Beta-Beads in the first and last run. The average conversion obtained with H-Beta-Beads over the 4 reaction runs was 91 %, with the highest and lowest conversions being 95 % and 86 %, respectively. The average conversion achieved with H-Beta-Pow over the 4 reaction runs was also 91 %. The selectivity of both catalysts remained nearly constant in the 79–83 % range throughout the reusability tests. Alto-

gether, these results demonstrate the high degree of reusability of H-Beta-Beads (and H-Beta-Pow) in consecutive runs.

Comparison between the catalytic performance of zeolite Beta beads, powder and extrudates as catalysts for the acylation of anisole in a fixed-bed reactor

In order to evaluate the potential of our binder-free zeolite Beta beads for larger-scale application, we tested their time-on-stream catalytic activity in continuous flow mode in a fixed-bed reactor. The catalyst lifetime is influenced by several factors in fixed-bed reactors, such as the flow rates of reactants, the removal of products from the reaction mixture and the pressure drop. To study the effects of the feed flow rate at atmospheric pressure, the three best catalysts identified in the previous section (H-Beta-Pow as reference catalyst, H-Beta-Beads and Beta70Kao30-Extr) were further tested in the acylation of anisole under continuous flow for 6 h in a fixed-bed set-up (see Experimental section). Beta70Kao30-Extr was chosen for this test even if it presented slightly lower activity than Beta90-Kao10-Extr in the batch-mode tests (Table 4), because the latter has poor mechanical stability due to its low binder content. In a preliminary test, three different liquid hourly space velocities (i.e. LHSV of 0.5, 1.0 and 1.5 $\text{g}_{\text{feed}} \cdot \text{min}^{-1} \cdot \text{g}_{\text{cat,bed}}^{-1}$) were investigated with H-Beta-Pow and H-Beta-Beads as the catalysts. In line with logical expectations, the conversion of acetic anhydride and the yield of p-MAP decreased by increasing the LHSV and thus decreasing the contact time between reactants and catalyst (Table 5, entries 1–3 and 4–6). Under all tested conditions, H-Beta-Pow was slightly more active than H-Beta-Beads, in agreement with the results obtained in batch mode (*vide supra*). It is worth noting that the drop in conversion between LHSV 0.5 and 1.0 $\text{g}_{\text{feed}} \cdot \text{min}^{-1} \cdot \text{g}_{\text{cat,bed}}^{-1}$ was much more significant over H-Beta-Pow (from 64 to 42%, Table 5, entries 1–2) than over H-Beta-Beads (from 40 to 32%, Table 5, entries 4–5). The intermediate LHSV (1 $\text{g}_{\text{feed}} \cdot \text{min}^{-1} \cdot \text{g}_{\text{cat,bed}}^{-1}$) was selected for a time-on-stream investigation in which H-Beta-Pow, H-Beta-Beads, and Beta70Kao30-Extr were compared (Figure 11). Notably, H-Beta-Beads displayed slightly higher initial activity (i.e.

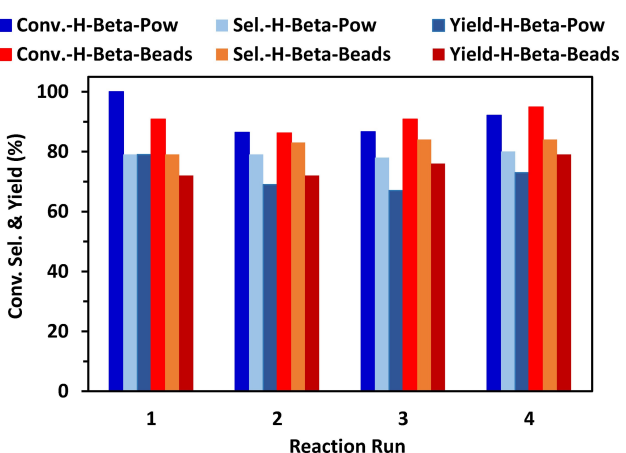
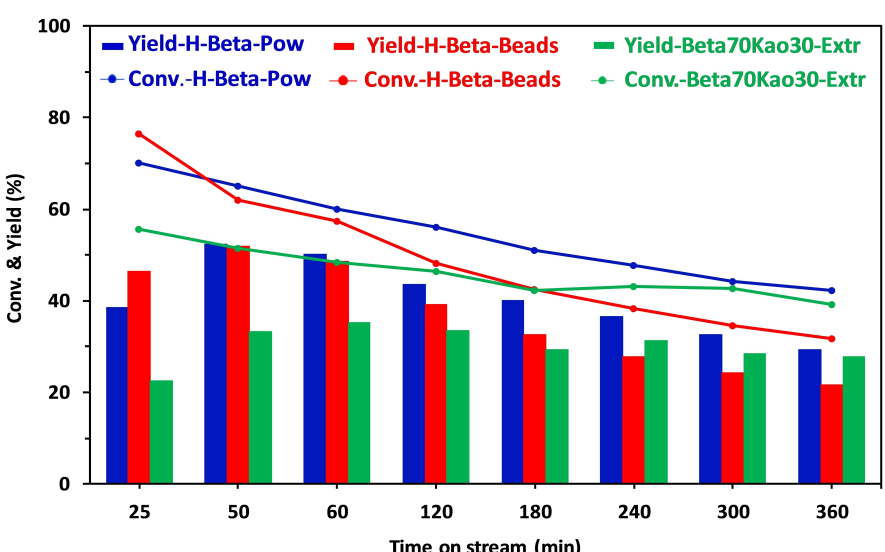


Figure 10. Reusability test of H-Beta-Beads and H-Beta-Pow in 4 consecutive batch runs. Reaction conditions: temperature = 90 °C, catalyst mass = 0.25 g, anisole = 50 mmol, acetic anhydride = 10 mmol (anisole to acetic anhydride molar ratio = 5:1), reaction time = 6 h.

Table 5. Catalytic performance of H-Beta-Pow, H-Beta-Beads and Beta70Kao30-Extr in the acylation of anisole in a fixed-bed reactor. The values provided in this table were measured after 6 h on stream.^[a]

Entry	Catalyst	LHSV [g _{feed} · min ⁻¹ · g _{cat, bed} ⁻¹]	Acetic anhydride Conv. [%] ^[b]	p-MAP Yield ^[c] [%]	p-MAP Sel. [%]	o-MAP Sel. [%]	Hydrolysis of acetic anhydride Sel. [%]
1	H-Beta-Pow	0.5	64	51	79	0	21
2	H-Beta-Pow	1.0	42	29	69	0	31
3	H-Beta-Pow	1.5	35	22	63	0	37
4	H-Beta-Beads	0.5	40	26	65	0	35
5	H-Beta-Beads	1.0	32	22	68	0	32
6	H-Beta-Beads	1.5	25	13	51	0	49
7	Beta70Kao30-Extr	1.0	39	28	71	0	29

[a] Reaction conditions: anisole to acetic anhydride molar ratio = 5:1, anisole to mesitylene molar ratio = 2:1, catalyst mass = 0.11 g, temperature = 90 °C, reaction time = 6 h. [b] The conversion was measured based on acetic anhydride, as this is the limiting reactant with the employed 5:1 ratio between anisole and acetic anhydride.

**Figure 11.** Comparison between the catalytic performance of H-Beta-Pow (blue), H-Beta-Beads (red) and Beta70Kao30-Extr (green) in a fixed-bed reactor at LHSV = 1.0 g_{feed} · min⁻¹ · g_{cat,bed}⁻¹. Reaction conditions as reported in Table 5.

within the first 50 min) compared to H-Beta-Pow and much higher than Beta70Kao30-Extr. However, the activity of H-Beta-Beads decreased more rapidly than that of the other two catalysts at longer time on stream, probably due to the adsorption of reaction products on the catalyst surface. This might be due to the higher hydrophilicity of H-Beta-Beads compared to H-Beta-Pow and Beta70Kao30-Extr (compare values of adsorbed H₂O molecule per surface unit in Table 1), which can lead to a higher degree of adsorption of acetic acid or other reaction products on the catalyst surface, thus causing faster deactivation.^[4,51,65] Nevertheless, over the tested 6 h range, the average p-MAP yield obtained over H-Beta-Beads was 37%, which is higher than that obtained over Beta70Kao30-Extr (30%). Future studies can be dedicated to understanding more in depth and minimizing the causes of deactivation of these catalysts.

Similarly to what was done for the test in batch mode (*vide supra*), the Weisz-Prater criterion was used to estimate if internal mass transfer limitation occurred in H-Beta-Beads when tested

in a fixed bed reactor. Also in this case, the calculated Weisz-Prater number is ≪ 1 (see SI for details), indicating that the reaction is not limited by internal diffusion.

Conclusions

In this study, three different binder-free zeolite beads (H-Beta-Beads, H-ZSM-5-Beads and H-Y-Beads) with hierarchical porous structure and macroscopic spherical format (d = 215–840 µm) were synthesized using commercially available anion-exchange Amberlite IRA-900 resin beads as hard template. A thorough physicochemical characterization with a combination of techniques demonstrated that the beads consist of interconnected crystalline zeolite particles that generate a hierarchical porous structure in which the micropores are accessible through a network of interparticle meso- and macropores. While a high degree of crystallinity was achieved in H-Beta-Beads and H-ZSM-5-Beads, the structure of H-Y-Beads was partially amor-

phous. Notably, all the zeolite beads displayed a larger ratio between Al atoms in tetrahedral and octahedral coordination compared to their counterpart zeolites prepared in powder format. The presence of both Lewis and Brønsted acid sites was evidenced in H-Beta-Beads by FTIR analysis of adsorbed pyridine. All the zeolite beads were tested as heterogeneous catalysts for the liquid-phase acylation of anisole using acetic anhydride in both batch and continuous flow reactors. Among all the catalytic beads, H-Beta-Beads showed the highest activity and selectivity in batch-mode tests (95% acetic anhydride conversion and 80% p-MAP selectivity after 6 h). This promising activity was coupled with a high reusability in four successive catalytic runs. H-Beta-Beads was also tested in continuous flow in a fixed-bed reactor using different LHSV, displaying excellent initial activity but gradually deactivating at longer time on stream. Overall, the activity of H-Beta-Beads was superior compared to extrudates prepared by mixing zeolite Beta powder with a binder (kaolin or bentonite), demonstrating the advantages of our binder-free catalysts. Future studies should be aimed at defining a regeneration procedure and at minimizing the deactivation of the zeolite beads when the acylation reaction is carried out in a fixed-bed reactor.

Experimental Section

Materials

Tetrapropylammonium hydroxide (TPAOH, 1.0 M in H_2O), tetraethylammonium hydroxide (TEAOH, 35 wt% in H_2O), tetramethylammonium hydroxide (TMAOH, 25 wt% in H_2O), silica gel (high purity grade 9385), anisole (99%), acetic anhydride (Reagent Plus, 99%), mesitylene (99%), 4-methoxyacetophenone (99%), Amberlite IRA-900 (with Cl^- as anions), 2-methoxyacetophenone (99%), acetic acid (Reagent Plus, 99%), bentonite ($\text{Al}_2\text{O}_{12}\text{Si}_4$) and kaolin ($\text{Al}_2\text{O}_5\text{Si}_2\cdot2\text{H}_2\text{O}$) were purchased from Sigma-Aldrich. Sodium aluminate anhydrous (purity 99.5%) was purchased from Riedel-de Haën. MilliQ water was used in all preparation steps in this work. All the above-mentioned chemicals for catalysts synthesis and catalytic reaction tests were applied without further purification.

Catalysts synthesis

The general procedure used to prepare the zeolite beads with hierarchical porosity reported in this work is shown in Figure 12.

ZSM-5 beads were prepared by adapting a protocol previously reported for the synthesis of ZSM-5 powder.^[66] In a typical synthesis, 4.58 g of silica gel was partially dissolved in 20.24 g of tetrapropylammonium hydroxide solution (TPAOH, 1 M solution in H_2O) and stirred at 100 °C for 1 h. Afterwards, a solution obtained by dissolving 0.64 g NaAlO_2 in 10.7 g H_2O upon stirring for 10 min was added dropwise (in ~10 min) to the first solution and then stirred for 1 h. Afterwards, the resin beads were directly added to the solution with a solution-to-bead mass ratio of 20:1.^[14] This mixture was transferred into a 50 ml Teflon-lined autoclave and the hydrothermal crystallization was carried out statically by placing the autoclave in an oven at 150 °C for 6 days. Next, the autoclave was allowed to cool down to room temperature and then opened. The obtained sample contained a mixture of powder and beads, which were separated from the liquid phase by filtration, washed with H_2O (1 L) until the pH reached approximately 7–8 and dried at 100 °C overnight in an oven. The dried ZSM-5 beads and the powder were separated by sieving on a sieve with an aperture size of 160 μm . The obtained beads consisted of a composite of crystalline ZSM-5 and Amberlite IRA-900 resin beads. In order to remove the resin template and the TPA⁺ used as micropore structure directing agent (SDA), calcination was performed with a two-step temperature program in a muffle furnace in static air from ambient temperature to 200 °C at 3 °C/min, 6 h at 200 °C, from 200 °C to 600 °C at 2 °C/min, 6 h at 600 °C. The same calcination protocol was used to remove the TPA⁺ from the powder samples. The obtained ZSM-5 beads and powder were in their sodium form. In order to convert both beads and powder to their H-form, the materials were suspended in a 1 M NH_4NO_3 solution (10 ml of solution per each gram of zeolite) at 80 °C for 8 h under stirring. Afterwards, the materials were washed with H_2O to reach pH around 7–8 and then dried at 100 °C overnight and calcined with the same temperature program applied for the first calcination step. These beads and powders were labeled as H-ZSM-5-Beads and H-ZSM-5-Pow, respectively.

Zeolite Beta beads were prepared by modifying an established hydrothermal synthesis procedure for the preparation of zeolite Beta powder.^[67] First, 4.58 g of silica gel was partially dissolved in 17.71 g of tetraethylammonium hydroxide solution (TEAOH, 35 wt% in H_2O) and stirred at room temperature for 1 h. Next, a second solution was prepared by dissolving 0.57 g NaAlO_2 in 10.74 g H_2O upon stirring for 10 min, and then added dropwise to the first solution followed by stirring for 1 h. Afterwards, the Amberlite IRA-900 resin beads were added to this solution in an amount corresponding to one-twentieth of the mass of the solution.^[14] The obtained mixture was transferred into a Teflon-lined 50 ml autoclave and hydrothermally crystallized at 150 °C for 6 days. The following steps of the synthesis were carried out with a similar procedure to that employed for the ZSM-5 beads (see

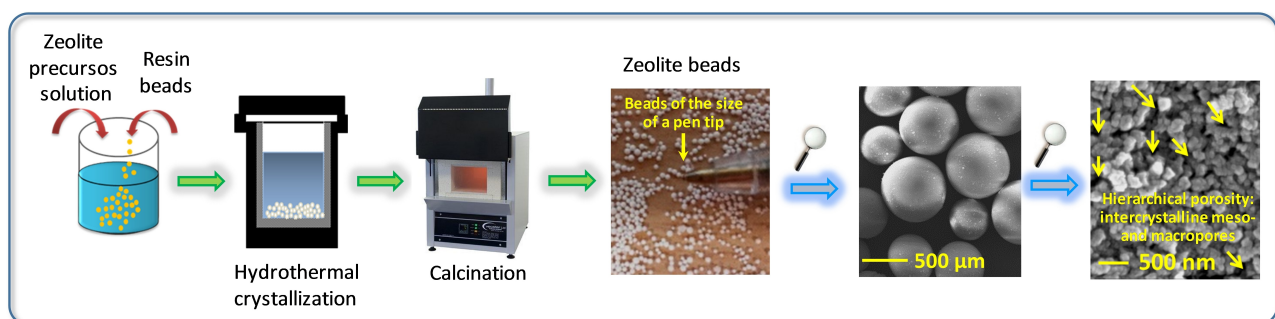


Figure 12. Procedure employed for the synthesis of zeolite beads using resin beads as hard templates (here, the H-Beta-Beads sample is shown).

above). The H-form Beta beads and powder were denoted as H-Beta-Beads and H-Beta-Pow, respectively.

Zeolite Y powder is generally synthesized without using any kind of organic SDA (e.g. quaternary ammonium salts). However, the SDA-free methods described in the literature^[68] were not successful in producing zeolite Y in bead format with a high degree of crystallinity. Although a series of experiments was performed in which several synthetic parameters such as temperature, mass ratio of polymeric beads, aging time and hydrothermal treatment conditions (e.g. temperature and time) were varied, only amorphous or partially crystalline beads possessing high mechanical strength were produced (see Figure S1). Therefore, a new synthesis route was developed by using tetramethylammonium hydroxide (TMAOH, 25 wt% in H₂O) as SDA for the micropores with the purpose of producing zeolite Y beads with higher degree of crystallinity. In a typical synthesis, 15 g TMAOH aqueous solution, 15 g H₂O and 2 g NaOH were mixed and stirred until NaOH was completely dissolved in the mixture. Then, 1.45 g NaAlO₂ was gradually added to the solution, followed by further stirring for 1 h. Finally, 3 g of silica gel was added in small portions to the mixture, which was further stirred for 30 min.^[69] Next, Amberlite IRA-900 beads were added to the mixture with the same mass ratio as in the aforementioned synthesis recipes (20:1) and this mixture was transferred to a Teflon bottle. The bottle was tightly closed with a screw cap and the mixture was aged for 7 days at room temperature under static conditions. Afterwards, hydrothermal treatment was conducted with a two-step temperature program. First, the Teflon bottle was placed into an oven at 50 °C for 48 h and then the temperature was increased to 100 °C with a ramp of 1 °C/min, and kept for 30 h at this temperature.^[69] The following steps of the synthesis were carried out as for the ZSM-5 beads (see above). Using this recipe, the final crystallinity of bead-shaped zeolite Y was significantly increased. The beads and powder of this sample were labeled as H-Y-Beads and H-Y-Pow, respectively. The best (i.e. most crystalline) bead sample obtained in the absence of SDA was labeled as H-Y-Beads-SC, in which SC indicates the semi-crystalline nature of the beads. The powder sample obtained together with H-Y-Beads-SC was highly crystalline zeolite Y (labelled as H-Y-powder-no-SDA, see Figure S1).

Zeolite Beta extrudates were prepared by mixing the lab-made zeolite Beta powder (H-Beta-Pow) with two types of clay binders (kaolin or bentonite) using a lab-scale extruder. Various relative masses of the binders (10, 30 and 50 wt% on the basis of dry mass ratios) were used. In order to increase the pastiness of the noodles passing through the extruder chamber, empirical amounts of H₂O were added to the zeolite-clay mixture. These extrudates were produced using an extruder die with an outer aperture diameter of 0.5 mm. After drying at 100 °C, the extruded noodles were calcined with the above-mentioned calcination program for ZSM-5 and, next, were cut into the appropriate length (average length of 1–2 mm, see Figure S2). The extrudates were labeled as BetamKaon-Extr and BetamBenn-Extr in which “Kao” and “Ben” are indicating kaolin and bentonite, respectively. The “m” and “n” suffixes are referring to the dry mass percentages applied for Beta powder and binders, respectively.

Catalytic tests

Anisole acylation using catalysts in powder form (H-Beta-Pow, H-ZSM-5-Pow, H-Y-Pow) was carried out in batch mode using a 48-well block heating plate under stirring at 800 rpm. Highly crystalline zeolitic beads (i.e. H-Beta-Beads, H-ZSM-5-Beads and H-Y-Beads) do not withstand stirring rates higher than 350 rpm using a magnetic stirring bar (i.e. they turn into powder). The tendency toward disintegration of the macroscopic structure under this stirring

mode was even more acute for the binder-containing extrudates, indicating that the latter have lower mechanical strength compared to our binder-free zeolite beads. To tackle this issue, we used a lab-made rotating vial instead of employing a stirring bar for the agitation of the reaction mixtures in the case of beads and extrudates. In such a set-up, a mechanical stirrer was connected to the reaction vial, which was then placed in an oil bath for heating (Figure S3). Using this system, all catalytic beads and extrudates remained fully intact throughout the catalytic test.

In a typical batch reaction, 50 mmol anisole, 10 mmol acetic anhydride, 25 mmol mesitylene (internal standard) and 0.25 g catalyst (in powder, bead or extrudate form) were loaded in a 15 ml glass vial and the reaction was performed at 90 °C and atmospheric pressure under vigorous stirring or rotation (800 rpm) for 6 h. To highlight better the differences in catalytic performance and lifetime of different catalysts, another set of batch reactions was conducted with lower catalysts loading, i.e. employing one-eighth of the previous catalyst mass (i.e. 31 mg), while using half of the above-mentioned reactant quantities (i.e. 25 mmol anisole, 5 mmol acetic anhydride, 12.5 mmol mesitylene) and a shorter reaction time (2.5 h). The main product of this reaction was para-methoxyacetophenone (p-MAP) in all cases. However, traces of ortho-methoxyacetophenone, o-MAP with low selectivity (<1%) was observed in some cases (Scheme 1).

Anisole is not only a reactant but also acts as a solvent in this liquid-phase reaction and help remove the adsorbed products from the zeolite surface. This can prevent rapid deactivation and thus increase the catalyst lifetime. Therefore, in all the catalytic tests an anisole-to-acetic-anhydride molar ratio of 5:1 was employed. After each batch-mode reaction using catalysts in powder form, the catalyst was separated from the mixture by filtration. In contrast, beads and extrudates immediately and spontaneously settled at the bottom of the reaction vial after turning off the mechanical rotation, without any need for further separation steps.

For the reusability tests, H-Beta-Pow and H-Beta-Beads were selected and examined in 4 consecutive runs in batch reactor mode. After each run, the collected catalyst from the reaction mixture was washed with 25 ml acetone and then 25 ml water to remove the residue of adsorbed products from the catalyst. This step was repeated three times. Afterwards, the catalyst was dried at 100 °C overnight and calcined at 550 °C (with the aforementioned temperature ramp). The amount of reaction solution for the second, third and fourth run was recalculated based on the recovered amount of catalyst after the calcination step performed for the removal of carbonaceous adsorbed products.

For continuous-flow tests, a bench-scale fixed-bed reactor was used. The in-house built set-up consists of a programmable single syringe pump (NE-1000, Swagelok), stainless steel tubings (length: 45 cm), a stainless steel fixed-bed reactor (length: 24 mm, inner diameter: 4 mm), two on-off valves, a pressure indicator, a K-type thermocouple mounted on the reactor wall and an internal thermocouple inside the catalyst bed (see Figure 13). The syringe pump was connected to the fixed-bed reactor through the inlet pipeline equipped with an on-off valve and the reactants were pumped into the reactor using a downward flow mode. A pressure indicator was installed before the fixed-bed reactor. All temperatures were controlled using a CN616 OMEGA PID temperature controller and OMEGA SYNC software with an error range of ±0.5 °C. Samples were taken from the bottom of the reactor at different time intervals via an on-off needle valve. The whole system was heated using heating tapes connected to the PID controller to set the bed temperature at 90 °C. In addition, the feeding lines and all connectors in the direction toward the reactor were insulated with ceramic fiber blankets located on the top of

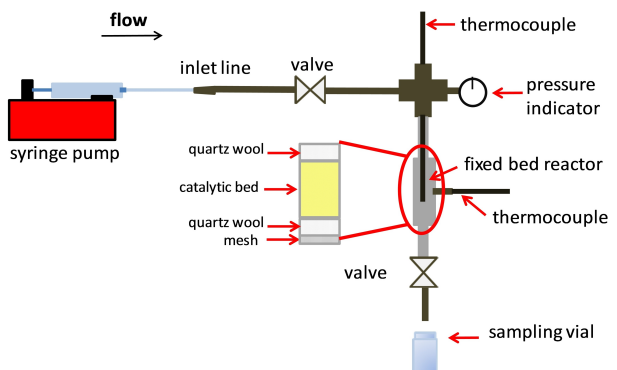


Figure 13. Schematic representation of the fixed-bed reactor set-up used for the catalytic acylation of anisole.

the heating tapes. For preparing the catalytic bed, a mesh was fixed at the bottom of the reactor and a thin layer of quartz wool was placed on the top of the mesh. Next, the bed was filled with 0.11 g of the chosen catalyst and, finally, another thin layer of quartz wool was placed on the top of the catalytic bed. The filled reactor was connected to the thermocouple from top and to the sampling valve from the downside.

Prior to the catalytic reaction and in order to make sure that there was no leakage in the set-up, the whole system was pressurized to 9 bar with N₂, kept overnight at this pressure and next depressurized to ambient pressure by opening the sampling valve at the bottom of the system. In order to start the reaction, the whole set-up was gradually heated up to 90°C. Next, the reaction was conducted by stepwise feeding the liquid-phase reactants to the catalytic bed with the same molar ratios like in the batch tests (i.e. anisole: acetic anhydride: mesitylene: 5:1:2). At the initial step, the inlet line was filled at a volumetric flow rate of 1 ml/min using a 60 ml syringe (inner diameter of 28.45 mm) and preheated for 15 min. Following this, the inlet and outlet valves of the reactor were opened and the catalytic bed was filled at the same flow rate until the first drop of liquid was observed in the sampling vial. Thereafter, the flow rate was switched to the desired quantity and the reaction time was measured from this point as time zero. Samples were taken at different intervals and analyzed by GC-FID. Three different Liquid Hourly Space Velocities (LHSV) of 0.5, 1, and 1.5 g_{feed}·min⁻¹·g_{cat,bed}⁻¹ (where g_{feed}·min⁻¹=ρ_{feed}·ml_{feed}·min⁻¹, in which ml_{feed}·min⁻¹ is the experimental value of the feed flow and ρ_{feed} is the estimated density of the feed, ρ_{feed}=Σρ_ix_i, in which ρ_i is the density of each of the three feed components (i.e. anisole, acetic anhydride and mesitylene) and x_i is the mass fraction of each feed component) were chosen for the fixed-bed studies.

At the end of the batch-mode reactions and at certain time intervals for the fixed-bed set-up, the reaction mixture was analyzed by gas chromatography (Agilent Technologies 7980B GC) equipped with an Agilent DB-5#6 (5%-phenyl)-methylpolysiloxane column (15 m length, 320 μm ID) and FID detector. GC calibration curves for all reactants and products were obtained using 4 different concentrations of the pure chemicals.

The conversion was measured based on acetic anhydride (being the limiting reactant) using Equation (1) and determined by sampling and injection into GC at the end of the reactions (e.g. after 2.5 or 6 h) for batch-mode reactions and by periodic sampling for fixed-bed tests:

$$\text{Conv.}_{\text{AA}} = \frac{\text{AA}_n - \text{AA}_0}{\text{AA}_0} \times 100 \% \quad (1)$$

in which AA₀ is the initial number of moles of acetic anhydride while AA_n is the number of moles of acetic anhydride at the end of batch-mode reactions and at the chosen sampling times for fixed-bed tests.

The selectivity toward para-methoxyacetophenone (p-MAP) as the main product and ortho-methoxyacetophenone (o-MAP) as the by-product of the acylation reaction were calculated based on Equation (2) and (3), respectively:

$$S_{\text{p-MAP}} = \frac{p\text{-MAP}}{\text{AA}_n - \text{AA}_0} \times 100 \% \quad (2)$$

$$S_{\text{o-MAP}} = \frac{o\text{-MAP}}{\text{AA}_n - \text{AA}_0} \times 100 \% \quad (3)$$

in which p-MAP and o-MAP are the moles of these two products at the end of batch-mode reactions and at the chosen sampling times for the tests in the fixed-bed reactor.

The yield of p-MAP and o-MAP were calculated using Equation (4) and (5), respectively:

$$Y_{\text{p-MAP}} = S_{\text{p-MAP}} \times \text{Conv.}_{\text{AA}} \quad (4)$$

$$Y_{\text{o-MAP}} = S_{\text{o-MAP}} \times \text{Conv.}_{\text{AA}} \quad (5)$$

The carbon balance was calculated based on the sum of the unreacted amounts of anisole and acetic anhydride at the end of the reaction, determined by GC-FID, plus the amounts of all detected products measured by GC-FID (i.e. p-MAP, o-MAP and acetic acid).

One mole of acetic acid is formed as side-product for each mole of acetic anhydride used to produce p-MAP or o-MAP through the acylation reaction (Scheme 1). As a competitive reaction, acetic anhydride can also hydrolyze into acetic acid, in which case two moles of acetic acid are obtained from each mole of acetic anhydride. The selectivity toward the (unwanted) hydrolysis of acetic anhydride was calculated using Equation 6:

$$S_{\text{AA}}(\text{hydrolysis}) = \frac{(\text{AAc} - p\text{-MAP} - o\text{-MAP})/2}{\text{AA}_0 - \text{AA}_n} \times 100 \% \quad (6)$$

in which AAc are the moles of acetic acid at the end of batch-mode reactions and p-MAP, o-MAP, AA₀ and AA_n are as defined above.

Selected tests were performed in duplicate, and showed good reproducibility. In such cases, the average of the conversion and yields are reported.

Characterization of the catalysts

X-ray diffraction patterns (XRD) were measured on a Bruker D-8 Advance-Spectrometer, with Cu-Kα radiation of λ=1.5418 Å generated at 40 kV and 40 mA. The 2θ angle data was collected from 5 to 50° with a step size of 0.02° and a scan rate of 1°·min⁻¹. Before analyzing samples using XRD, the zeolite beads were ground into powder. The hierarchical structure was investigated by scanning electron microscopy (SEM) using a Philips XL30 ESEM FEG equipment. Prior to SEM and due to the non-conductive nature of

zeolites, all beads and powders were coated with gold. Nitrogen physisorption was measured on a Micromeritics ASAP 2420 apparatus at -196°C . The specific surface area was measured using the Brunauer-Emmet-Teller (BET) model and the mesopores size distribution was calculated by the Barret-Joyner-Halenda (BJH) model on the desorption branch of the physisorption curve. Transmission electron microscopy (TEM) images were taken using a CM12 (Philips) electron microscope working at 120 keV. Prior to TEM analysis, the beads were gently ground into powders. TEM samples were prepared by suspension of different powder samples in ethanol by sonication for 40 min. Next, one drop of the prepared suspension was placed on a TEM 400 mesh copper grid with a carbon coating. Elemental analysis was performed by X-ray fluorescence (XRF) using a PANalytical Epsilon 3XL instrument. In a typical analysis, 100 mg of a zeolite sample was measured in a plastic cup equipped with a mylar film. The amount of each element was calculated assuming that the elements are in their oxide forms. The hydrophilicity of selected samples was estimated by thermogravimetric analysis (TGA) on a Perkin Elmer TGA 4000 instrument under N_2 atmosphere using a heating rate of $10^{\circ}\text{C}\cdot\text{min}^{-1}$. The zeolite samples were previously saturated to their maximum water capacity through water adsorption overnight in a desiccator containing a saturated aqueous solution of NH_4Cl . The number of water molecules ($n_{\text{H}_2\text{O}}$) adsorbed per nm^2 of surface area of zeolite was calculated from the mass loss between 25 and 300°C using the following equation: $n_{\text{H}_2\text{O}} = \frac{\Delta m}{m_i} \times \frac{N_A}{A_{\text{BET}}M_{\text{H}_2\text{O}}}$, where Δm is the mass loss per gram of zeolite between 25 and 300°C (i.e. the temperature at which all TGA plots had reached a plateau, see Figure S4); m_i is the initial mass of the sample at 25°C (in grams). N_A is the Avogadro constant ($6.022 \times 10^{23} \text{ mol}^{-1}$). A_{BET} is the specific surface area of the sample (in $\text{nm}^2\cdot\text{g}^{-1}$); $M_{\text{H}_2\text{O}}$ is the molar mass of water ($18.0153 \text{ g}\cdot\text{mol}^{-1}$). In addition, selected used catalysts were analyzed by TGA under air atmosphere (heating rate: $10^{\circ}\text{C}\cdot\text{min}^{-1}$) to quantify the deposition of carbonaceous species. The Si/Al molar ratio and Al coordination in different zeolitic frameworks were measured by solid-state NMR (nuclear magnetic resonance) spectroscopy. All measurements were carried out on a Bruker Biospin Avance Neo NMR spectrometer equipped with a 14.1 T magnet and a 4 mm broadband magic angle spinning (MAS) probe. The corresponding Larmor frequency for ^{27}Al and ^{29}Si was 156.375 and 119.229 MHz, respectively. All measurements were conducted in 4 mm zirconia rotors (Bruker Biospin) at a spinning rate of 12.5 kHz and 293 K temperature. ^{27}Al single pulse experiments were done with a 2 μsec pulse length, 2 sec repetition delay, 5120 scans. ^{29}Si single pulse experiments were done with a 90° pulse corresponding to nutation frequency 42.5 kHz and in the case of zeolite Y samples 62.5 kHz, 256 sec repetition delay, and 256 scans. Spectra were measured using the Bruker Topspin program and peak deconvolution was performed using the DMFit program.^[70] The Si/Al molar ratio was calculated using the following equation:

$$\frac{\text{Si}}{\text{Al}} = \frac{400}{\sum_{n=0}^4 n I_{\text{Si}(n\text{Al})}}, \quad [43]$$

where I is the relative integrated signal intensity of various Si(nAl) units [e.g. Si(0Al), Si(1Al), Si(2Al), Si(3Al) and Si(4Al)], with n being the number of adjacent Al nuclei.^[43] The Brønsted and Lewis acid amounts were measured by pyridine adsorption monitored by FT-IR using a Bruker Vertex 70 spectrophotometer equipped with a liquid nitrogen-cooled mercury-cadmium-telluride (LN-MCT) detector operating at 4 cm^{-1} resolution. Thin self-supporting discs were prepared by pressing approximately 30 mg of each sample (disc diameter $\sim 1 \text{ cm}$) and next outgassed under vacuum at 200°C for 1 h before pyridine adsorption. The spectra of chemisorbed pyridine desorption were recorded at 150, 350 and 450°C for 30 min with a heating rate of $4^{\circ}\text{C}/\text{min}$.

Acknowledgements

We acknowledge Léon Rohrbach for analytical support and Dr. Zhenchen Tang for help with acquiring the TEM images. We are also thankful to Shell plc for their support for the pyridine FT-IR measurements. We acknowledge Hero Goldhoorn for his guidance on the extrusion technique.

Conflict of Interest

The authors declare no conflict of interest.

Data Availability Statement

The data that support the findings of this study are available from the corresponding author upon reasonable request.

Keywords: Extrudates • Friedel-Crafts • Hierarchical porosity • Zeolite Beta • Zeolite beads

- [1] M. Guidotti, J. M. Coustard, P. Magnoux, M. Guisnet, *Pure Appl. Chem.* **2007**, *79*, 1833–1838. doi:10.1351/pac200779111833.
- [2] K. M. Parida, S. Rana, S. Mallick, D. Rath, *J. Colloid Interface Sci.* **2010**, *350*, 132–139. doi:10.1016/j.jcis.2010.06.025.
- [3] H. Wei, S. Xie, N. Gao, K. Liu, X. Liu, W. Xin, X. Li, S. Liu, L. Xu, *Appl. Catal. A* **2015**, *495*, 152–161. doi:10.1016/j.apcata.2015.02.020.
- [4] Z. Chen, Y. Feng, T. Tong, A. Zeng, *Appl. Catal. A* **2014**, *482*, 92–98. doi:10.1016/j.apcata.2014.05.028.
- [5] M. L. Kantam, K. V. S. Ranganath, M. Sateesh, K. B. S. Kumar, B. M. Choudary, *J. Mol. Catal. A* **2005**, *225*, 15–20. doi:10.1016/j.molcata.2004.08.018.
- [6] G. Sartori, R. Maggi, *Chem. Rev.* **2006**, *106*, 1077–1104. doi:10.1021/cr040695c.
- [7] B. Chiche, A. Finiels, C. Gauthier, P. Geneste, J. Graille, D. Pioch, *J. Org. Chem.* **1986**, *51*, 2128–2130. doi:10.1021/jo00361a039.
- [8] P. B. Venuto, *Microporous Mesoporous Mater.* **1994**, *2*, 297–411. doi:10.1016/0927-6513(94)00002-6.
- [9] M. G. Clerici, *Top. Catal.* **2000**, *13*, 373–386. doi:10.1023/A:1009063106954.
- [10] Y. Tao, H. Kanoh, L. Abrams, K. Kaneko, *Chem. Rev.* **2006**, *106*, 896–910. doi:10.1021/cr0402040.
- [11] L. Tosheva, V. P. Valtchev, *Chem. Mater.* **2005**, *17*, 2494–2513. doi:10.1021/cm047908z.
- [12] D. P. Serrano, J. M. Escola, P. Pizarro, *Chem. Soc. Rev.* **2013**, *42*, 4004–4035. doi:10.1039/c2cs35330j.
- [13] C. C. Freyhardt, M. Tsapatis, R. F. Lobo, K. J. Balkus, M. E. Davis, *Nature* **1996**, *381*, 295–298. doi:10.1038/381295a0.
- [14] W. Cheng, Y. Jiang, X. Xu, Y. Wang, K. Lin, P. P. Pescarmona, *J. Catal.* **2016**, *333*, 139–148. doi:10.1016/j.jcat.2015.09.017.
- [15] J. Pérez-Ramírez, C. H. Christensen, K. Egeblad, C. H. Christensen, J. C. Groen, *Chem. Soc. Rev.* **2008**, *37*, 2530–2542. doi:10.1039/b809030k.
- [16] K. Möller, T. Bein, *Chem. Soc. Rev.* **2013**, *42*, 3689–3707. doi:10.1039/c3cs35488a.
- [17] C. Madsen, C. J. H. Jacobsen, *Chem. Commun.* **1999**, *8*, 673–674. doi:10.1039/a901228a.
- [18] M. Choi, H. S. Cho, R. Srivastava, C. Venkatesan, D. H. Choi, R. Ryoo, *Nat. Mater.* **2006**, *5*, 718–723. doi:10.1038/nmat1705.
- [19] D. Verboekend, T. C. Keller, S. Mitchell, J. Pérez-Ramírez, *Adv. Funct. Mater.* **2013**, *23*, 1923–1934. doi:10.1002/adfm.201202320.
- [20] C. J. H. Jacobsen, C. Madsen, J. Houzvicka, I. Schmidt, *J. Am. Chem. Soc.* **2000**, *122*, 7116–7117. doi:10.1021/ja000744c.
- [21] M. Gackowski, K. Tarach, L. Kuterasiński, J. Podobiński, S. Jarczewski, P. Kuśkowski, J. Datka, *Microporous Mesoporous Mater.* **2018**, *263*, 282–288. doi:10.1016/j.micromeso.2017.11.051.

- [22] S. Yang, C. Yu, L. Yu, S. Miao, M. Zou, C. Jin, D. Zhang, L. Xu, S. Huang, *Angew. Chem. Int. Ed.* **2017**, *56*, 12553–12556; *Angew. Chem.* **2017**, *129*, 12727–12730. doi:10.1002/anie.201706566.
- [23] K. Egeblad, C. H. Christensen, M. Kustova, C. H. Christensen, *Chem. Mater.* **2008**, *20*(3), 946–960. doi.org/10.1021/cm702224p.
- [24] T. Pan, Z. Wu, A. C. Yip, *Catalysts* **2019**, *9*(3), 274. doi.org/10.3390/catal9030274.
- [25] M. C. Silaghi, C. Chizallet, P. Raybaud, *Microporous Mesoporous Mater.* **2014**, *191*, 82–96. doi:10.1016/j.micromeso.2014.02.040.
- [26] N. L. Michels, S. Mitchell, J. Pérez-Ramírez, *ACS Catal.* **2014**, *4*, 2409–2417. doi:10.1021/cs500353b.
- [27] G. T. Whiting, S. H. Chung, D. Stosic, A. D. Chowdhury, L. I. Van Der Wal, D. Fu, J. Zecevic, A. Travert, K. Houben, M. Baldus, B. M. Weckhuysen, *ACS Catal.* **2019**, *9*, 4792–4803. doi:10.1021/acscatal.9b00151.
- [28] L. Tosheva, V. Valtchev, J. Sterte, *Microporous Mesoporous Mater.* **2000**, 35–36, 621–629. doi:10.1016/S1387-1811(99)00256-5.
- [29] L. Tosheva, J. Sterte, *Stud. Surf. Sci. Catal.* **2002**, *142*, 183–189, doi:10.1016/S0167-2991(02)80027-1.
- [30] L. Tosheva, B. Mihailova, V. Valtchev, J. Sterte, *Microporous Mesoporous Mater.* **2001**, *48*, 31–37, doi:10.1016/S1387-1811(01)00327-4.
- [31] V. Naydenov, L. Tosheva, J. Sterte, *Stud. Surf. Sci. Catal.* **2002**, *142*, 1449–1455, doi:10.1021/cm0211507.
- [32] V. Naydenov, L. Tosheva, J. Sterte, *Chem. Mater.* **2002**, *14*, 4881–4885. doi:10.1021/cm0211507.
- [33] K. Lin, O. I. Lebedev, G. Van Tendeloo, P. A. Jacobs, P. P. Pescarmona, *Chem. Eur. J.* **2010**, *16*, 13509–13518. doi:10.1002/chem.201001508.
- [34] Z. Asgar Pour, D. G. Boer, S. Fang, Z. Tang, P. P. Pescarmona, *Catalysts* **2021**, *11*, 1346–1360. doi:10.3390/catal11111346.
- [35] Y. A. Alasmmy, Z. Asgar Pour, P. P. Pescarmona, *ACS Sustainable Chem. Eng.* **2020**, *8*, 7993–8003. doi:10.1021/acssuschemeng.0c02265.
- [36] E. G. Derouane, I. Schmidt, H. Lachas, *Catal. Lett.* **2004**, *95*, 13–17. doi:10.1023/B:CATL.0000023715.41857.56.
- [37] Z. Yang, Y. Xia, R. Mokaya, *Adv. Mater.* **2004**, *16*, 727–732. doi:10.1002/adma.200306295.
- [38] M. B. J. Roeffaers, R. Ameloot, M. Baruah, H. Uji-i, M. Bulut, G. De Cremer, U. Müller, P. A. Jacobs, J. Hofkens, B. F. Sels, D. E. De Vos, *J. Am. Chem. Soc.* **2008**, *130*, 5763–5772. doi:10.1021/ja7113147.
- [39] P. Botella, A. Corma, J. M. López-Nieto, S. Valencia, R. Jacquiot, *J. Catal.* **2000**, *195*, 161–168. doi:10.1006/jcat.2000.2971.
- [40] S. Musić, N. Filipović-Vinceković, L. Sekovanić, *Braz. J. Chem. Eng.* **2011**, *28*, 89–94. doi:10.1590/S0104-66322011000100011.
- [41] C. Berger, R. Gläser, R. A. Rakoczy, J. Weitkamp, *Microporous Mesoporous Mater.* **2005**, *83*, 333–344. doi:10.1016/j.micromeso.2005.04.009.
- [42] C. Danumah, S. Vaudreuil, L. Bonneviot, M. Bousmina, S. Giasson, S. Kalaguine, *Microporous Mesoporous Mater.* **2001**, *44*–*45*, 241–247. doi:10.1016/S1387-1811(00)00287-0.
- [43] A. G. Stepanov, *Basics of Solid-State NMR for Application in Zeolite Science: Material and Reaction Characterization*, Elsevier B. V., 2016. doi:10.1016/B978-0-444-63506-8.00004-5.
- [44] E. Sellie, L. Froni, *Microporous Mesoporous Mater.* **1999**, *31*, 129–140, doi:10.1016/S1387-1811(99)00063-3.
- [45] M. Maache, A. Janin, J. C. Lavalle, *Zeolites* **1993**, *13*, 419–426. doi:10.1016/0144-2449(93)90114-1.
- [46] M. Guisnet, P. Ayayit, C. Coutanceau, M. Fernanda Alvarez, J. Datka, *J. Chem. Soc. Faraday Trans.* **1997**, *93*(8), 1661–1665, doi:10.1039/A607609B.
- [47] C. A. Emeis, *J. Catal.* **1993**, *141*, 347–354. doi:10.1006/jcat.1993.1145.
- [48] X. Rao, H. Ishitani, W. J. Yoo, S. Kobayashi, *Asian J. Org. Chem.* **2019**, *8*(3), 316–319, doi:10.1002/ajoc.201900012.
- [49] H. L. Hsu, R. Selvin, T. M. Her, *J. Therm. Anal. Calorim.* **2007**, *89*, 379–383. doi:10.1007/s10973-006-8155-4.
- [50] J. Stelzer, M. Paulus, M. Hunger, J. Weitkamp, *Microporous Mesoporous Mater.* **1998**, *22*, 1–8. doi:10.1016/S1387-1811(98)00071-7.
- [51] D. Rohan, C. Canaff, E. Fromentin, M. Guisnet, *J. Catal.* **1998**, *177*, 296–305. doi:10.1006/jcat.1998.2108.
- [52] U. Freese, F. Heinrich, F. Roessner, *Catal. Today.* **1999**, *49*, 237–244. doi:10.1016/S0920-5861(98)00429-5.
- [53] K. Smith, Z. Zhenhua, P. K. G. Hodgson, *J. Mol. Catal. A* **1998**, *134*, 121–128. doi:10.1016/S1381-1169(98)00028-4.
- [54] R. Kore, R. Srivastava, B. Satpati, *Appl. Catal. A* **2015**, *493*, 129–141. doi:10.1016/j.apcata.2015.01.002.
- [55] J. C. Kim, K. Cho, S. Lee, R. Ryoo, *Catal. Today.* **2015**, *243*, 103–108. doi:10.1016/j.cattod.2014.07.055.
- [56] I. Sreedhar, H. Kantamneni, K. Suresh Kumar Reddy, K. V. Raghavan, *Kinet. Catal.* **2014**, *55*, 229–232. doi:10.1134/S0023158414020116.
- [57] K. Gaare, D. Akporiaye, *J. Mol. Catal. A* **1996**, *109*, 177–187. doi:10.1016/1381-1169(96)00023-4.
- [58] A. Padmanabhan, R. Selvin, H.-L. Hsu, L. W. Xiao, *Chem. Eng. Technol.* **2010**, *33*, 998–1002. doi:10.1002/ceat.200900542.
- [59] H. Smail, M. Rehan, K. Shareef, Z. Ramli, A. S. Nizami, J. Gardy, *ChemEngineering.* **2019**, *3*, 35. doi:10.3390/chemengineering3020035.
- [60] R. Selvin, H. L. Hsu, T. M. Her, *Catal. Commun.* **2008**, *10*, 169–172. doi:10.1016/j.catcom.2008.08.013.
- [61] A. K. Pandey, A. P. Singh, *Catal. Lett.* **1997**, *44*, 129–133. doi:10.1023/A:1018964722746.
- [62] G. T. Whiting, A. D. Chowdhury, R. Oord, P. Paalanen, B. M. Weckhuysen, *Faraday Discuss.* **2016**, *188*, 369–386. doi:10.1039/C5FD00200A.
- [63] H. Faghihian, N. Godazandeha, *J. Porous Mater.* **2009**, *16*, 331–335, doi:10.1007/s10934-008-9204-0.
- [64] M. L. M. Bonati, R. W. Joyner, M. Stockenhuber, *Microporous Mesoporous Mater.* **2007**, *104*, 217–224. doi:10.1016/j.micromeso.2007.02.023.
- [65] E. G. Derouane, C. J. Dillon, D. Bethell, S. B. Derouane-Abd Hamid, *J. Catal.* **1999**, *187*, 209–218. https://doi.org/10.1006/jcat.1999.2575.
- [66] R. J. Argauer, G. R. Landolt, Crystalline Zeolite ZSM-5 and Method of Preparing The Same, US Patent 3,702,886 (1972).
- [67] R. L. Wadlinger, G. T. Kerr, E. J. Rosinski, Catalytic composition of a crystalline zeolite, US Patent 3,308,069 (1967).
- [68] D. W. Breck, Crystalline Zeolite Y, US Patent 3,130,007 (1964).
- [69] D. Karami, N. Mahinpey, *Can. J. Chem. Eng.* **2014**, *92*, 671–675. doi:10.1002/cjce.21902.
- [70] D. Massiot, F. Fayon, M. Capron, I. King, S. L. e Calvé, B. Alonso, J. O. Durand, B. Bujoli, Z. Gan, G. Hoatson, *Magn. Reson. Chem.* **2002**, *40*, 70–76. doi:10.1002/mrc.984.

Manuscript received: April 16, 2022

Revised manuscript received: June 23, 2022

Accepted manuscript online: July 6, 2022

Version of record online: August 3, 2022